Double pulse laser-induced breakdown spectroscopy for the analysis of plasma-facing components

J. Oelmann, E. Wüst, G. Sergienko, S. Brezinsek

Forschungszentrum Jülich GmbH - Institut für Energie- und Klimaforschung - Plasmaphysik, Partner of the Trilateral Euregio Cluster (TEC), 52425 Jülich, Germany

E-mail: j.oelmann@fz-juelich.de

Abstract. Laser-induced breakdown spectroscopy is applied successfully for plasma-wall interaction studies in several fusion devices and post-mortem analyses of plasma-facing materials. However, the quantitative as well as qualitative analysis of low hydrogen isotope contents in tungsten plasma-facing components is still challenging. A promising approach to increase the optical signal in laser-induced breakdown spectroscopy is to apply a second laser pulse to the laser-produced plasma. We present two setups for post mortem plasma-facing component analyses using different laser pulse properties and different excitation geometries. The enhancement factors and changes in spectral line shapes for double pulse compared to single pulse laser-induced breakdown spectroscopy are presented.

Keywords: Double pulse laser-induced breakdown spectroscopy, Plasma-Facing Components, Fuel retention, Laser based diagnostics
Submitted to: *Phys. Scr.*

1. Introduction

Laser-induced breakdown spectroscopy (LIBS) is a measurement technique for composition analysis of materials and used in various research as well as industrial fields [1]. Compared to many other common analytical techniques, LIBS analysis is rapid and the measurement does not require sample preparation. It can be applied remotely and with high distance to the target and thus also in complex and, regarding measurements, challenging environments.

Many factors influence the laser-produced plasma emission, like laser properties (pulse duration, wavelength and fluence), the ambient gas and pressure, light collection optics and the detectors [2]. In order to increase the signal-to-noise-ratio of LIBS, for example to detect low amounts of trace element in materials, within the past years the so called double pulse laser-induced breakdown spectroscopy (DP-LIBS) became an established approach [3]. The main mechanism in this approach is that after a first laser pulse, which ablates target material and induces a plasma, a second laser pulse is used to heat the generated plasma and, thus, increase emitted radiation. Consequently, for DP-LIBS not only the interaction of the laser pulse with a target needs to be optimized, but the laser-plasma interaction must be taken into account. In terms of selecting laser pulse properties for DP-LIBS, it was shown that emissions of the plasma are higher if the pulse duration of the first laser pulse is shorter than the pulse duration of the second laser pulse [4]. Moreover, a higher energy of the second laser pulse compared to the first laser pulse shows higher signal enhancement factors [5]. In all DP-LIBS applications, the time dependent expansion of the laser-produced plasma from the first laser pulse requires to match the inter-pulse delay of the laser pulses to the plasma position.

One application field for LIBS is plasma-facing component (PFC) analysis as fuel retention diagnostics in fusion research [6, 7]. Also DP-LIBS was used for in-situ analyses in fusion devices with an robotic arm and for post-mortem measurements in laboratories [8]. Still, the detection of low amounts of hydrogen isotopes retained in metallic PFCs remains to be challenging. Retention analyses were mainly presented utilizing laser pulse durations in the nanosecond range [9]. Although these ns-laser systems are widely used nowadays, heat penetration into the target caused by the laser pulse limits the depth resolution, especially for gaseous species in measurements of metals with high thermal conductivity. Consequently, we propose to apply laser pulses with pulse durations in the order of picoseconds for depth resolved measurements [10]. This manuscript presents new measurement setups for ps-DP-LIBS analyses of PFCs with different excitation geometries, pulse duration variations and an optimization of the inter-pulse delay. Section 2 gives an overview of the two experimental setups used for DP-LIBS. Details to the PFCs are given in section 3, anal-

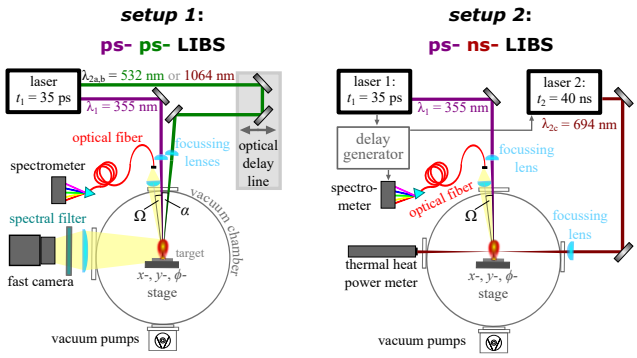

Figure 1. Schematic overview of the setups for DP-LIBS, each using a laser with pulse durations of $t_1 = 35$ ps at a wavelength of $\lambda_1 = 355$ nm for plasma induction at the targets surface in a vacuum chamber. The plasma can be heated by a second laser pulse with different pulse properties and different optical beam paths. Emitted light is analyzed in two spectrometers and with a fast camera.

yses and discussion regarding the different laser pulse parameters are presented in section 4. A summary and outlook is given in section 5.

2. Experimental setups for DP-LIBS

For the analyses shown in section 4, two experimental setups for post-mortem PFC analyses are used, combining different lasers as well as laser beam paths. Schematic overviews of the setups are shown in Figure 1. For laser-induced ablation of the PFCs and plasma induction on its surface, the third harmonic of a Nd:YAG laser by *EKSPLA* with a pulse duration of $t_1 = 35$ ps is focused by means of a plano-convex quartz lens with a focus length of $f = 500$ mm to a laser spot diameter of $d_1 = 750\,\mu$m on a tungsten target in a vacuum chamber. The base pressure before ablation is 2×10^{-5} Pa. The laser pulse energy is $E_1 = 30$ mJ for all laser-induced ablations. The ablation rate per laser pulse of $\mathrm{d}h = 30$ nm is in the same order of magnitude as the heat penetration depth of the ultra short laser pulses, enabling depth resolved measurements [10]. The emitted radiation is collected in quasi-coaxial direction to the beam path of this laser pulse ($\Delta\Omega = (5 \pm 2.5)^\circ$) by two quartz lenses, guided through single core optical fibers and analyzed in an echelle spectrometer (*ESA4000* by *LLA instruments*) as well as a self build high resolution spectrometer [11] equipped with a fast gated *Andor iStar 334* camera. Details to this single pulse LIBS (SP-LIBS) setup can be found in recent publications [12, 13]. In the following, expansions of this setup are presented for DP-LIBS in collinear as well as in orthogonal geometry of the two laser pulses. They are termed according to the pulse duration regime of the first and second laser pulse respectively.

2.1. ps-ps-LIBS setup

In addition to the third harmonic ($\lambda_1 = 355$ nm, $E_1 \leq 30$ mJ), the Nd:YAG laser provides spatially separated outputs of laser pulses with $\lambda_{2a} = 532$ nm, $E_{2a} \leq 10$ mJ and $\lambda_{2b} = 1064$ nm, $E_{2b} \leq 40$ mJ. In the first of the presented DP-LIBS setups, one of these laser pulses is focused with another plano-convex quartz lens (focusing length $f = 500$ mm) on the laser-produced plasma of the first laser pulse after passing an optical delay line of up to 15 m. The beam diameter at the plasma is $\approx 700\,\mu$m with a focus position 25 mm in front of the target. The length of the delay line determines the inter-pulse delay, which we limit to 50 ns to maintain a reasonable number of reflections with resulting losses at the optical components as well as laser beam divergence. The angle between the first and second laser pulse is ($\Delta\alpha = 5^\circ$) due to the dimensions of the two focusing lenses. With respect to the plasma plume, this can be seen as approximately collinear. This excitation geometry can also be applied *in-situ* in fusion devices. The properties of the second laser pulse are fixed to $E_2 = 39$ mJ and $\lambda_{2b} = 1064$ nm for measurements shown in section 4.1.
For an analysis of the target, emitted radiation of the laser-produced plasma is analyzed with the two spectrometers stated above. Additionally, an observation parallel to the targets surface with a fast camera enables to analyze the plasma expansion. A narrow band pass filter (central wavelength: $\lambda_C = 656.1$ nm, spectral width $\Delta\lambda_{1/2} = 2$ nm) is used to analyze the D_α radiation. Time resolved measurements of the plasma plume expansion offer information for a spacial and temporal overlap for the DP-LIBS measurements in orthogonal geometry described in the following subsection.

2.2. ps- ns- LIBS setup

The second setup for DP-LIBS uses the same laser with picosecond pulse duration as first laser pulse. To heat the laser-produced plasma, here a ruby laser ($\lambda_{2c} = 694$ nm, $E_{2c} \leq 1500$ mJ) with a pulse duration of 40 ns is used. Thus, the provided pulse energies are much higher compared to ps-ps-LIBS in *setup 1*. The pulse duration of the second laser pulse is still lower than the lifetime of the plasma in vacuum. To avoid thermal heating of the PFC with the second high power laser pulse, an orthogonal excitation is chosen like shown in Figure 1. The beam diameter at the plasma is 1.5 mm and a 2 mm distance of the second laser pulse to the tungsten target surface is chosen. Laser radiation which is not absorbed by the plasma passes a vacuum window and is measured with a thermal heat power meter. The inter-pulse delay is set by a digital delay generator (*DG645* by *Stanford R.S.*).

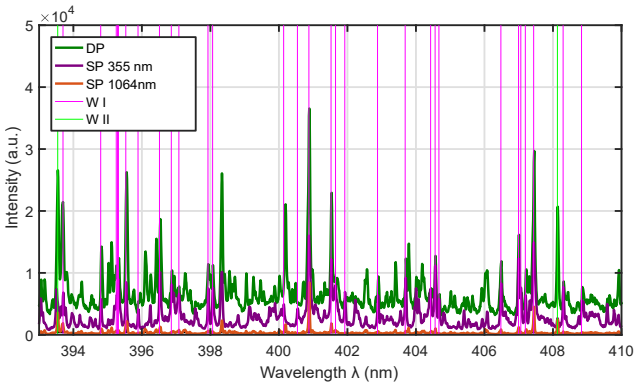

Figure 2. Spectra of a tungsten target taken with *setup 1* for ps-ps-LIBS, SP-LIBS applying $\lambda = 355\,\text{nm}$ and SP-LIBS applying $\lambda = 1064\,\text{nm}$. W spectral line positions from NIST database are shown as vertical lines[16].

The enhancement factor of DP- compared to SP-LIBS for different inter-pulse delay times is analyzed in section 4.

3. Samples

To induce conditions relevant to fusion edge plasma, tungsten samples with a high purity of 99.99 wt.% W are exposed to deuterium ions in the linear plasma device PSI-2 [14]. Before the plasma exposure, the samples were mechanically polished and annealed at 1273 K for three hours. The ion flux during plasma exposure was kept at $2.9 \times 10^{21}\ \text{D}^+\text{m}^{-2}\text{s}^{-1}$ for five hours, giving a total fluence of $5.0 \times 10^{25}\ \text{D}^+\text{m}^{-2}$. The surface temperature was 500 K. The retained amount of deuterium in the targets is in the order of 10^{19} D atoms/m^2 according to laser-induced ablation quadrupole mass spectrometry analyses (LIA-QMS, measurement technique described in [15]).

4. Results and discussion

4.1. Enhancement factors in collinear ps-ps-LIBS

At first, W spectral line emission is analyzed with DP-LIBS in collinear excitation geometry applying laser pulses of two wavelength from the same laser (see *setup 1* in Figure 1). The inter pulse delay for all spectra shown in this subsection is fixed at 50 ns. Figure 2 shows measurements for ps-ps-LIBS, SP-LIBS applying $\lambda = 355\,\text{nm}$ and SP-LIBS applying $\lambda = 1064\,\text{nm}$. 50 spectra of a laser-produced plasma at a pure tungsten target surface are accumulated, each recorded at a delay time of 100 ns with respect to plasma formation induced by the first laser pulse. The gate width is 110 ns. W atomic and ionic spectral line positions from NIST database are shown as vertical lines[16]. The laser pulse energies are $E_1 = 30\,\text{mJ}$ for $\lambda = 355\,\text{nm}$ and $E_2 = 39\,\text{mJ}$ for $\lambda = 1064\,\text{nm}$ for all measurements, resulting in a total applied energy of $E_{DP} = 69\,\text{mJ}$ in the DP-LIBS case. Although the pulse energy is lower, the measurement intensities for SP-LIBS are higher for $\lambda = 355\,\text{nm}$ than for $\lambda = 1064\,\text{nm}$ due to the higher photon energy and thus a more efficient ablation and plasma generation. As expected, the detected intensity for DP-LIBS is even higher than the sum of both SP-LIBS spectra in the whole observed wavelength range. Voigt profiles are fitted to the spectra to determine the area under the spectral lines, labeled *spectral line intensity* in the following. To compare the signal enhancement factor, consequently the sum of the SP-LIBS measurements intensities are compared to the DP-LIBS signals:

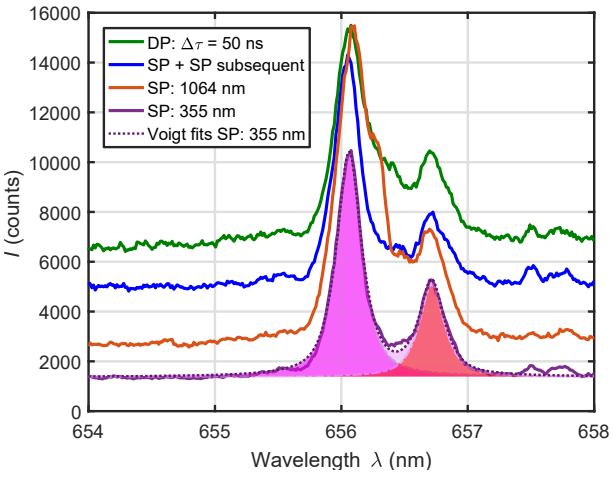

Figure 3. Spectra of a deuterium exposed tungsten target for LIBS measurements with the same color code like in Figure 2. The additional blue curve shows the sum of two spectra taken in subsequent measurements at the same target position with SP-LIBS of both wavelengths.

$$\frac{I_{\text{DP}}}{I_{\text{SP}}} = \frac{I_{\text{DP}}}{I_{355\,\text{nm}} + I_{1064\,\text{nm}}}. \tag{1}$$

The highest measurement signal in the wavelength range shown in Figure 2 is observed for the W I transition at 400.875 nm ($5\text{d}^5(^6\text{S})6\text{p} \rightarrow 5\text{d}^5(^6\text{S})6\text{s}$). The enhancement factor for this spectral line intensity is $\frac{I_{\text{DP}}}{I_{\text{SP}}}(400.875\,\text{nm}) = 1.4$. Note that the continuum background emission, which is enhanced by a factor of 2.7 in DP-LIBS for this delay time, is taken as an offset for the voigt profile fit and thus not included in the spectral line intensity enhancement factor. Other atomic and ionic lines are amplified by factors of up to 2.6, showing that for the W I transition at 400.875 nm the coefficient of spontaneous emission A_{ki} is so high, that self-absorption in the LIBS plasma occurs.

Figure 3 shows LIBS spectra from single pulse measurement of a tungsten target which was exposed to deuterium ions. Each line shown is referring to a new position at the targets surface to compare

equivalent target concentrations. The blue line in Figure 3, labeled *"SP+SP (subsequent)"*, shows the sum of SP-LIBS spectra with the second ablation in the laser-induced crater of the first laser pulse. A slightly lower peak intensity than for the DP-LIBS spectrum is observed. Due to a Doppler shift of the emitted radiation of the light and thus fast ablated hydrogen and deuterium atoms, D_α ($\lambda = 656.1\,\mathrm{nm}$) and H_α ($\lambda = 656.3\,\mathrm{nm}$) spectral radiation is shifted to lower wavelength λ. Also a second peak with lower intensity is observed at higher wavelength, resulting from radiation emitted in direction of the target, which is then partially reflected at its surface before reaching the spectrometer. Two voigt function fits are shown for one spectrum of single pulse LIBS for visualization of this hydrogen spectral line splitting. The parasitic hydrogen content is assigned to adsorption of water on the target surface when exposed to air after deuterium implantation (shown LIBS analyses are not performed in the linear plasma device PSI-2). The two peak positions at $\lambda = 656.0\,\mathrm{nm}$ and $\lambda = 656.7\,\mathrm{nm}$ show, that mainly H_α radiation is observed. The D_α line intensity is much lower than this parasitic H_α radiation (and reflection) for this sample with a deuterium retention of 10^{19} D atoms/m^2 and cannot be separated for these measurements.

To efficiently heat the laser induced plasma in DP-LIBS, the laser spot diameter of the $\lambda = 1064\,\mathrm{nm}$ laser pulse is chosen higher than the $\lambda = 355\,\mathrm{nm}$ laser pulse. This leads to a laser-induced crater on the target with a diameter of $d_2 = 950\,\mu\mathrm{m}$. Thus, the illuminated area is 60% higher for the $\lambda = 1064\,\mathrm{nm}$ laser pulse and a larger hydrogen intensity is observed in Figure 3. Although the continuum background signal is significantly enhanced in DP-LIBS, the hydrogen line spectral intensity is not amplified. A possible explanation for the missing spectral line intensity enhancement is that the light hydrogen atoms are ablated with a higher velocity and occupy a larger volume then the tungsten atoms so that the second laser pulse interacts with a small fraction of the induced plasma only.

To exclude the interaction of the second laser pulse with the target, section 4.2 describes DP-LIBS measurements in orthogonal excitation geometry.

4.2. Line broadening in orthogonal ps-ns-LIBS

For DP-LIBS with laser pulses from different lasers, like "*setup 2*" shown in Figure 1, the inter-pulse delay Δt is not limited by the length of an optical delay line but can be set by a digital delay generator. Figure 4 shows the enhancement factor of a W I spectral line for a 2 mm distance of the second laser pulse to the tungsten target surface. The exposure of the spectrometer is set to $5\,\mu\mathrm{s}$ without a gate delay

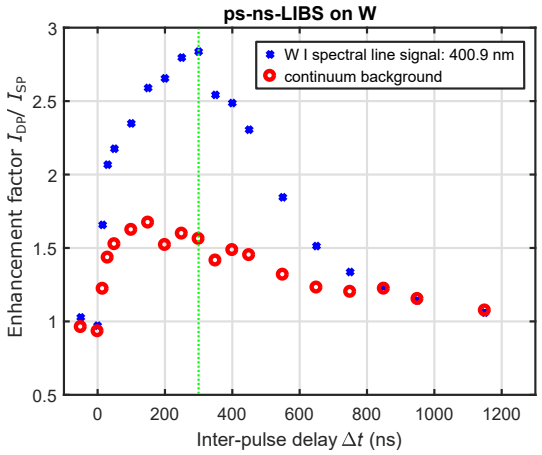

Figure 4. ps-ns-LIBS enhancement factor of an atomic W spectral line and the continuum background radiation for different inter pulse delays Δt analyzed for tungsten target ablation in *setup 2*.

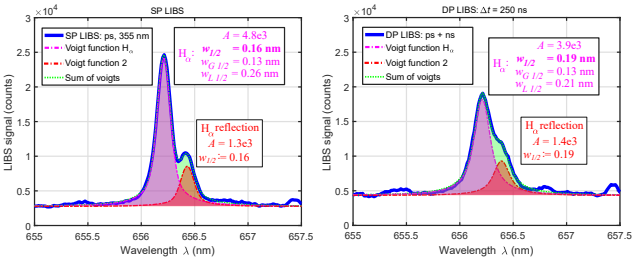

Figure 5. Voigt function fits with determined total line widths $w_{1/2}$ and line widths of Lorentzian $w_{L1/2}$ and $w_{G1/2}$ and Gaussian functions for H_α radiation and its reflection in SP- and ps-ns-LIBS measurements.

to ensure that the emission is not delayed due to reheating of the plasma by the second laser pulse. The amplification of the W I spectral line ($\lambda = 400.875\,\mathrm{nm}$) is rising up to an inter-pulse delay of $\Delta t = 300\,\mathrm{ns}$ and falling for higher delays. The continuum background radiation enhancement factor is dropping already after $\Delta t = 160\,\mathrm{ns}$. Figure 5 shows spectra of a deuterium exposed tungsten target for SP- and DP-LIBS.

Like in the optical range around 400 nm shown in Figure 4, also at 655 nm the continuum background intensity is significantly (57%) higher for DP-LIBS. However, the detected H_α spectral intensity is 19% lower than for SP-LIBS, whereas the total line width at half maximum $w_{1/2}$ rises by 17%. The plasma density N_e, determined from stark broadening of the H_α spectral lines [1] are N_e(SP-LIBS) $= 1.6 \times 10^{16}\,\mathrm{cm}^{-3}$ and N_e(DP-LIBS) $= 2.0 \times 10^{16}\,\mathrm{cm}^{-3}$. Consequently, also for a DP-LIBS configuration in orthogonal excitation geometry, H_α spectral line intensity enhancement could not be achieved by applying the same experimental settings and adjustments as for which an enhancement of W I spectral line intensity is observed.

5. Conclusion and outlook

Two double pulse laser-induced breakdown spectroscopy setups for post-mortem plasma-facing component analyses are presented and first measurement results of deuterium exposed tungsten are shown. Excitation geometries are compared regarding optical intensity enhancement of tungsten and hydrogen spectral lines. The short pulse duration of the first laser pulse in these setups keep the feature of a depth resolved PFC analysis. Measurements of single and double pulse-LIBS on tungsten show enhancement factors of 1.4–2.6 for atomic and ionic tungsten spectral line intensities. The spectroscopic H_α signal from water on the sample surface was too high to resolve the deuterium retention signal in the order of 10^{19} D atoms/m^2 for the first laser pulse. Although the hydrogen radiation is not significantly amplified in either excitation geometry, stark broadening analyses show an 25% higher plasma density in DP- compared to SP-LIBS and thus a clear interaction of the second laser pulse with the laser-induced plasma. This does not constitute DP-LIBS as a sensible method for post-mortem fuel retention studies of plasma-facing components, at least not for the applied experimental adjustments. Yet it demonstrates that enhancement factors of tungsten cannot be directly transferred to the amplification of hydrogen isotopic spectral lines in fuel retention studies. Further studies will investigate variations of the inter-pulse delay and optimization of the distance from the W:D target to the focus of the second laser pulse in orthogonal excitation geometry to optimize DP-LIBS for the measurement signal enhancement of radiation from deuterium deeper in the target for depth resolved analyses.

6. Acknowledgment

This work has been carried out within the framework of the EUROfusion Consortium and has received funding from the Euratom research and training programme 2014-2018 and 2019-2020 under grant agreement No 633053. The views and opinions expressed herein do not necessarily reflect those of the European Commission.

References

[1] S. K. Hussain Shah et al. *Radiat. Phys. Chem.* **170** 108666 (2020).

[2] S. Musazzi et al. *Springer Series in Optical Sciences* **182** (2014) ISBN 978-3-642-45084-6 .

[3] Y. Li et al. *Appl. Spectrosc. Rev.* **53** 1–35 (2018).

[4] Y. Wang et al. *Opt. Laser Technol.* **122**, 105887 (2020).

[5] R. Ahmed et al. *Laser Phys. Lett.* **12** 066102 (2015).

[6] S. Brezinsek et al. *Nucl. Fusion* **57** 116041 (2017).

[7] G. Maurya et al. *J. Nucl. Mater.* **541** 152417 (2020).

[8] A. Almaviva et al. *Fusion Eng. Des.* (*157* 111685 (2020).

[9] R. Fantoni et al. *Spectrochim. Acta Part B At. Spectrosc.* **129** 8–13 (2017).

[10] R. Yi et al. *Appl. Surf. Sci.* **532** 147185 (2020).

[11] G. Sergienko et al. *Fusion Eng. Des.* **123** 906–910 (2017).

[12] J. Oelmann et al. *Nucl. Mater. Energy* **26** 100943 (2021).

[13] D. Zhao et al. *Nucl. Fusion* **61** 016025 (2021).

[14] A. Kreter et al. *Fusion Science and Technology* **68** 8–14 (2015).

[15] J. Oelmann et al. *Spectrochim. Acta - Part B At. Spectrosc.* **144** 38–45 (2018).

[16] D. D. Laun et al. *J. Res. Natl. Bur. Stand. (U.S.)*, **A 72**, 609–755 (1968). NIST Atomic Spectra Database, available: https://physics.nist.gov/asd [2021, April 19].